Computers and Fluids 288 (2025) 106521

Contents lists available at ScienceDirect

Computers and Fluids

journal homepage: www.elsevier.com/locate/compfluid

LES study of turbulent flow fields over a three-dimensional steep hill considering the effects of thermal stratification

Tong Zhou, Takeshi Ishihara *

Department of Civil Engineering, School of Engineering, The University of Tokyo, 113-8656, Japan

ARTICLE INFO

Keywords:
Large-eddy simulation
Thermal stratification
Turbulent flow fields
Three-dimensional steep hill
Force balance analysis

ABSTRACT

In this study, large-eddy simulations are performed to elucidate the spatiotemporal characteristics and physical mechanisms of turbulent boundary layers over hilly terrain under stable, neutral, and unstable stratification. The impact of thermal stratification on turbulent flows over a steep three-dimensional hill is clarified through flow patterns and statistical characteristics. Compared to neutral stratification, the separation bubble downstream of the hill crest is reduced under unstable stratification, while it is enlarged under stable stratification. In addition, turbulent eddy motions in the wake region are enhanced in the unstable condition but are suppressed in the stable condition. Both mean velocities and turbulence fluctuations over steep hilly terrain are amplified by unstable stratification and attenuated by stable stratification. The flow characteristics on the hill crest are comprehensively determined by the topography and thermal stratification, whereas the flow dynamics in the hill wake are predominantly influenced by terrain-induced turbulence. Moreover, the mechanisms driving the formation of flow fields over steep hilly topography under different thermal stratification are investigated through force balance analysis using the time-averaged Navier–Stokes equations. The results indicate that turbulence plays a negligible role in the force balance upstream of the hill, while it becomes the dominant factor for the force balances downstream of the hill.

1. Introduction

To achieve carbon neutrality in 2050, an increasing number of wind farm projects have been initiated in mountainous regions worldwide. However, the complex atmospheric environment and intricate topographic features in these regions give rise to highly complicated interactions between the atmospheric boundary layer (ABL) and hilly terrain, leading to various challenging flow phenomena. To optimize the wind energy utilization in mountainous areas, a comprehensive understanding of turbulent flows over hilly terrain is paramount. Extensive efforts have been dedicated to elucidating the dominant features of turbulent boundary layers over hills through field measurements, laboratory experiments and numerical simulations.

For the purpose of revealing flow characteristics over real complex terrain, many full-scale observations have been carried out by using cup anemometers and wind vanes [21,47,57,67], as well as some remote sensing devices like LiDAR and SoDAR [7,8,30,35,48,72]. However, it is noteworthy that field measurements are subject to numerous uncontrollable factors and observed data are affected by meteorological conditions. In contrast to field measurements, laboratory experiments have the advantages of being fully controllable and highly reproducible. Additionally, wind tunnel tests can provide valuable information about flow dynamics and coherent turbulence structures over hills. Consequently, many experimental research have been performed to clarify the influence of various factors on flow fields over topography, including surface roughness [4,9–11,64], hill slopes [13,20,29,31,50] and hill shapes [22,25,27,55]. Nevertheless, there are some limitations due to the viscous distortions at low Reynold numbers [49]. Moreover, laboratory experiments cannot provide a comprehensive view of the flow field due to the restricted number of sampling points. Computational Fluid Dynamics (CFD) modelling has been increasingly utilized to analyze the characteristics of turbulent boundary layer over hilly terrain. In general, the flow behaviors and turbulence characteristics over mountainous areas are numerically investigated by two primary approaches: Reynolds-averaged Navier-Stokes (RANS) and large eddy simulation (LES). Owing to the favorable trade-off between the numerical fidelity and computational efficiency, two-equations RANS models have been broadly applied for modeling of atmospheric flows

* Corresponding author.
E-mail address: ishihara@bridge.t.u-tokyo.ac.jp (T. Ishihara).

https://doi.org/10.1016/j.compfluid.2024.106521
Received 24 August 2024; Received in revised form 29 November 2024; Accepted 8 December 2024
Available online 9 December 2024

over hilly terrain [6,20,23,24,26,31,32,44,46,75]. Nonetheless, it should be noted that steady RANS methods are deficient in accurately capturing the unsteady flow phenomena in the hill wake. On the other hand, due to the nature of time-dependent calculations, LES has greater potential for providing high-resolution spatio-temporal features of atmospheric flows over hills [12,14,15,18,19,28,39–42,65,66,76,78].

Although earlier studies thoroughly investigated turbulent flows over topography, most of these studies have relied on the neutral stratification assumption, which ignored the effects of buoyancy force caused by the temperature variations within the ABL. However, the neutral assumption cannot adequately represent the actual atmospheric environment. The thermal stability of ABL demonstrates a pronounced diurnal variation owing to the solar radiation. The stable stratification typically occurs at nighttime and the airflow is distinguished by the high wind shear and low turbulence intensity suppressed by buoyancy force, while the unstable condition is predominant during the daytime and the airflow is identified by the low wind shear and high turbulence intensity caused by vigorous turbulent mixing. The discrepancies of dominant forcing mechanisms in different thermally-stratified ABL flows can lead to large variations of flow pattern and turbulence statistics. Consequently, the neutral stratification assumption might lead to uncertainties and errors in wind flow modelling over mountainous terrain [33,38,58,60]. Nevertheless, only a few of experimental and numerical investigations have considered the effect of thermal stratification on turbulent flows over hilly terrain until now. Recently, the RANS-based flow solvers have been developed to incorporate the influence of atmospheric stability and demonstrated favorable improvement for mean wind speed predictions on the hilltop [3,5]. However, it is still questionable whether the RANS models can accurately predict turbulent statistics in the hill wake, which involve many unsteady flow phenomena. Moreover, the mechanism by which the flow fields are formed around hills under different thermal stratification is unclear. Previous studies have primarily focused on the effects of stable stratification on atmospheric flows over hills [33,37,59,69,71,77]. The impact of unstable stratification on turbulent flows over hills has been barely investigated, which may impede accurate wind resource assessment in complex terrain.

This study aims to provide a comprehensive analysis of the influence of thermal stratification on flow dynamics over a three-dimensional (3-D) steep hill. The numerical methods for predicting thermally-stratified ABL flows using the LES turbulence model are introduced in Section 2. The turbulence models are validated by the wind tunnel measurements over flat terrain and a 3-D steep hill under different thermal stratification in Section 3. The effects of thermal stratification on turbulent flow fields over a 3-D steep hill are subsequently discussed and the mechanisms governing the formation of flow fields are elucidated through force balance analysis in Section 4. Finally, the conclusions of the present study are summarized in Section 5.

2. Numerical methods

2.1. Governing equations

Thermally-stratified ABL flows over flat and hilly terrain are modelled using LES in this study. The governing equations are derived by utilizing a low-pass filter to the unsteady Navier–Stokes equations, which can be expressed as follows:

$$\frac{\partial \widetilde{u}_i}{\partial x_i} = 0 \tag{1}$$

$$\frac{\partial \widetilde{u}_i}{\partial t} + \frac{\partial \widetilde{u}_i \widetilde{u}_j}{\partial x_j} = \frac{\partial}{\partial x_j}\left(\frac{\mu}{\rho_0}\frac{\partial \widetilde{u}_i}{\partial x_j}\right) - \frac{1}{\rho_0}\frac{\partial \widetilde{p}}{\partial x_i} - \frac{\partial \tau_{ij}}{\partial x_j} + g_i[1-\beta(\widetilde{\theta}-\theta_0)] \tag{2}$$

$$\frac{\partial \widetilde{\theta}}{\partial t} + \widetilde{u}_j\frac{\partial \widetilde{\theta}}{\partial x_j} = \frac{\partial}{\partial x_i}\left(\frac{\nu}{Pr}\frac{\partial \widetilde{\theta}}{\partial x_j} - \tau_{\theta j}\right) \tag{3}$$

where the tilde "∼" stands for the spatial filtering operation, $u_i = (u,\ v,\ w)$ denotes the velocity components, $x_i = (x,\ y,\ z)$ represents the spatial coordinates in three orthogonal directions (longitudinal, lateral and vertical directions), μ and ν are the dynamic and kinematic viscosity, respectively, ρ_0 is the reference air density ($= 1.225\ \mathrm{kg/m^3}$), p is the non-hydrostatic pressure, β is the thermal expansion coefficient ($= 3.3 \times 10^{-3}\ \mathrm{K^{-1}}$), g_i is the gravitational acceleration ($= (0,\ 0,\ -9.81)\ \mathrm{m/s^2}$) and θ_0 is the reference temperature. Incorporating unresolved turbulent fluctuations on a resolved flow field, the subgrid-scale (SGS) stress τ_{ij} and SGS heat flux $\tau_{\theta j}$ are specified as:

$$\tau_{ij} = -2\mu_t\widetilde{S}_{ij} + \frac{1}{3}\delta_{ij}\tau_{kk} \tag{4}$$

$$\tau_{\theta j} = -\frac{\mu_t}{Pr_t}\frac{\partial \widetilde{\theta}}{\partial x_j} \tag{5}$$

where μ_t refers to the SGS eddy viscosity, $\widetilde{S}_{ij}$ denotes the resolved rate-of-strain tensor ($= \frac{1}{2}\left(\frac{\partial \widetilde{u}_i}{\partial x_j} + \frac{\partial \widetilde{u}_j}{\partial x_i}\right)$), δ_{ij} is the Kronecker delta, and Pr_t is the turbulent Prandtl number. The standard Smagorinsky model is employed for the parameterization of the SGS eddy viscosity as:

$$\mu_t = (C_s\Delta)^2|\widetilde{S}| \tag{6}$$

where C_s is the Smagorinsky constant ($= 0.1$), Δ is the grid-filter width ($= \left(\Delta_x\Delta_y\Delta_z\right)^{1/3}$), and $|\widetilde{S}|$ is the magnitude of the resolved strain-rate tensor ($= (2\widetilde{S}_{ij}\widetilde{S}_{ij})^{1/2}$). The explicit van Driest damping function $f = 1 - \exp(-y^+/25)$ is used to reduce the SGS eddy viscosity adjacent to the wall, as the standard Smagorinsky model is incapable of resolving the viscous sublayer.

Based on the Boussinesq hypothesis, the flow is assumed to be incompressible with a constant fluid density ρ_0 and variations in air density due to temperature changes are considered to only affect the buoyancy force. This approximation can significantly reduce the computational complexity associated with the density variations in all governing equations and satisfactory accuracy is maintained if the temperature differences are below the following threshold:

$$\beta(\theta - \theta_0) \ll 1 \tag{7}$$

The Boussinesq approximation has been widely adopted for numerical models of thermally-stratified ABL flows over flat terrain [34,53,54], building arrays [1,43,45] and wind farms (Porte-Agel et al., 2011; [2,63]).

2.2. Computational domain and grid system

The layout of LES simulations of thermally-stratified ABL flows over 3-D steep hills are shown in Fig. 1. Consistent with the wind tunnel experiments conducted by Ishihara et al. [27], several roughness blocks of varying heights (60 mm, 20 mm and 10 mm) are arranged in a staggered configuration upstream of the test section. To generate turbulent boundary layer flows, the numerical wind tunnel approach is adopted in this study and roughness blocks are explicitly resolved using fine computational grids. Additionally, an additional buffer region with a length of 2.0 m is implemented upstream of roughness blocks with the aim of eliminating the negative impact of unphysical perturbations from the inlet plane. The hill model is set 3.4 m from the turbulence generation region, in which a fully developed turbulent boundary layer is reproduced. Moreover, the outlet of the computational domain is placed 2.4 m downstream of the hill model, with the aim of minimizing the influence on the target area from the outlet. In engineering applications, several inflow turbulence generation methods have also been proposed and discussed by Wu [73], Dhamankar et al. [17], Thordal et al. [68] in detail.

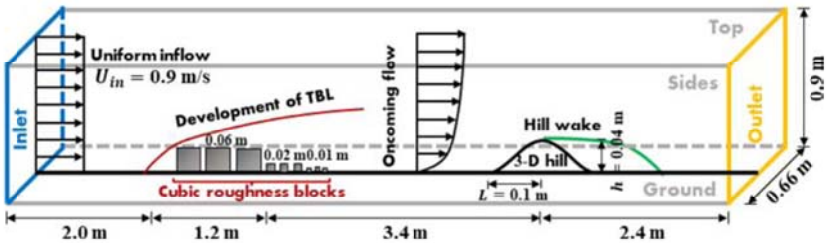

Fig. 1. Layout of the numerical wind tunnel for thermally-stratified ABL flows over a 3-D steep hill.

In this study, the geometric shape of the 3-D steep hill is defined by the following equations:

$$z_s = \begin{cases} h\cos^2\pi\left(x^2+y^2\right)^{1/2}\Big/2L, & \left(x^2+y^2\right)^{1/2} < L \\ 0, & \left(x^2+y^2\right)^{1/2} \geq L \end{cases} \tag{8}$$

where L is the base radius of the 3-D steep hill ($L = 100$ mm) and h is the hill height ($h = 40$ mm). The maximum slope of the hill model considered in this study is approximately 32°, which is sufficiently steep to induce flow separation downwind of the hill.

To attain an optimal trade-off between numerical accuracy and efficiency, a nested grid system is applied around the steep terrain, as illustrated in Fig. 2(a). The fine grid domain covers $22.5h \times 5h \times 22.5h$ in the x (longitudinal), y (lateral) and z (vertical) directions, respectively. To mitigate the influence of gradual changes in the grid spacing on the hill model, the length of the upstream fine grid area is set to $12.5h$, which is greater than that of the downstream region. In the fine grid area, various horizontal grid resolutions ranging from 10 mm to 1 mm are examined to guarantee that the underlying flow physics can be correctly captured while maintaining computational efficiency. Since the simulations with horizontal resolutions of 2 mm and 1 mm almost yield the same results, implying that a horizontal grid size of 2 mm is sufficient for accurate predictions of turbulent flows over steep terrain. Additionally, a small buffer zone is stretched around the central fine-grid area with a stretching rate of 1.2 to provide a smooth grid transition to the rough grid region. For the rough grid region, square-shaped cells with a horizontal grid resolution of 10 mm are used. Moreover, the terrain-following grid system as depicted in Fig. 2(b) is adopted in the vertical direction to improve the vertical resolution near curved terrain for better predictions of terrain-induced turbulence. The minimum vertical grid spacing is 0.2 mm nearest to the ground, and the maximum stretching ratio is 1.1. The value of y^+ on the ground surface ranges from 0.5 to 1.0. The total quantity of cells in the optimal grid system in this study is approximately 7.3 million.

2.3. Boundary conditions

Regarding the boundary conditions, the inlet is subject to Dirichlet conditions for the velocity and temperature and a Neumann condition for the pressure. A uniform inflow velocity U_∞ of 0.9 m/s is imposed at the inlet. In order to account for the effects of thermal stratification, a piecewise linear temperature profile is prescribed upstream of the roughness blocks. The outlet is specified as a pressure-outlet boundary condition, in which the gradients of all physical variables except pressure are set to zero. Symmetric boundary conditions are employed for lateral sides of the computational domain. The free-slip condition is used in the upper boundary, while the no-slip condition with wall function is applied to the lower boundary. The boundary conditions for LES simulations of thermally-stratified turbulent flows over a steep hill are given in Table 1.

The Reynolds number ($Re = U_h h/\nu$) in this study is approximately 1.2×10^4, matching that of the wind tunnel tests performed by Ishihara et al. [27]. To maintain the same Reynolds number level, the air viscosity is proportionally reduced in response to a six-fold reduction in the

Table 1
Boundary conditions for thermally-stratified ABL flows over a steep hill.

Locations	Boundary conditions
Inlet	Dirichlet condition for velocity and temperature: $u = 0.9$ m/s, $v = w = 0$ $\theta(K) = \begin{cases} 285.15 + 100\,z & z < 0.6 \\ 345.15 + 33(z-0.6) & 0.6 \leq z < 1.0 \end{cases}$ (SBL) $\theta(K) = \begin{cases} 288.15 & z < 0.21 \\ 288.15 + 500(z-0.21) & 0.21 \leq z < 0.33 \\ 348.15 + 33(z-0.33) & 0.33 \leq z < 1.00 \end{cases}$ (CBL) Neumann condition for pressure: $\partial p/\partial n = 0$
Outlet	Dirichlet condition for p; Neumann condition for u, v, w, θ
Spanwise sides	Symmetric condition
Top	Free slip condition for u, v, w; Neumann condition for p, θ
Bottom	No-slip condition for u, v, w; Neumann condition for p; Dirichlet condition for θ_s: θ_s = 282.15 K (SBL); θ_s = 343.15 K (CBL)

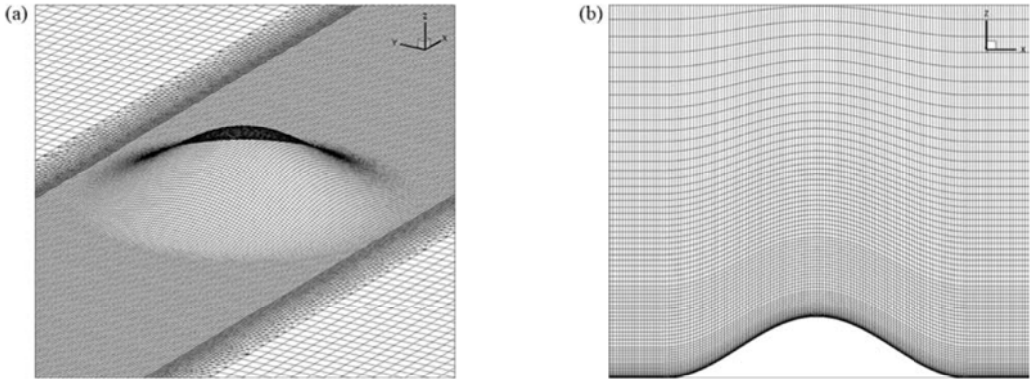

Fig. 2. Grid arrangement around a 3-D steep hill: (a) bird view and (b) side view.

inlet wind speed compared to the wind tunnel. Note that this strategy has been carefully validated by Qian et al. [56] and this study to ensure its feasibility. In addition, thermal effects are not significantly affected by the Reynolds number. The effects of topography and thermal stratification can be separated for predicting the mean wind speed in complex terrain, which was validated using full-scale measurement data from a wind farm located in the North of Japan by Yamaguchi et al. [74].

2.4. Numerical schemes and solution strategies

The finite volume method is adopted for unsteady LES calculations, in which all flow variables are allocated over an unstructured grid system. Regarding the numerical discretization of the governing equations, the linear-upwind stabilized transport (LUST)scheme is utilized for the convective term of momentum equations and the Gauss limited linear scheme is applied to the convective term of the temperature equation. The Gauss linear scheme with explicit non-orthogonal correction is used for the diffusion term. In addition, the implicit backward scheme is used to discretize the unsteady term in the governing equations. To deal with the iterative procedures of coupling equations for velocity and pressure, the PIMPLE algorithm, a combination of the PISO and SIMPLE algorithms, is selected for the present study due to its robustness and stability. The time increment Δt is set to 0.001 s, ensuring that the maximum CFL number remains below 1 in the target area during each iteration. Different algebraic solvers are used for the solution of velocity, temperature and pressure equations. The stabilized preconditioned bi-conjugate gradient (PBiCGStab) solver with the diagonally incomplete-LU-pre-conditioner (DILU) is adopted to solve the velocity and temperature equations. The generalized geometric-algebraic multi-grid (GAMG) solver is employed for solving the pressure equation. The convergence criteria are specified as the initial residual for all flow variables dropping below 10^{-6}. In this study, all simulations are conducted for 45 s and the first 15 s are used to stabilize the transient flow field. The sampling duration is determined by examining the relative errors of turbulent statistics at a reference point ($x = 3.75h$, $y = 0$, $z = h$) in the wake region. The relative discrepancies of mean velocities and turbulence fluctuations became <5 % when the sampling time reached 30 s. All simulations are conducted using a parallel computing system with 112 cores and 512 GB memory (Intel Xeon CPU E5–2667 v4 @ 3.20 GHz), taking approximately 132 h to run each case. The numerical schemes adopted in the LES simulations are outlined in Table 2.

3. Model validation

The validation of the present study is structured into two major parts. The first part evaluates the performance of the LES model in simulating different thermally stratified boundary layer flows. To be specific, atmospheric flows over flat terrain under stable and unstable stratification are examined in Section 3.1 and 3.2, respectively. The second part assesses the accuracy of the LES model in predicting turbulent flows over steep hilly terrain, which will be presented in detail in Section 3.3.

3.1. ABL flows over flat terrain under stable stratification

To generate the stable boundary layer (SBL), the vertical temperature profile of the incoming flow is pre-shaped by a heating unit and the ground temperature is cooled to around 9 °C. The computational domain extends over dimensions of 11 H (length) × 0.5 H (width) × 1.0 H (height), as illustrated in Fig. 3. Regarding the mesh arrangement, a background mesh with a uniform horizontal grid spacing of 0.01 H (H = 1m) and vertical grid stretching ratio of 1.05 is generated using the structured blockMesh application. Additionally, a local grid refinement scheme is adopted in the proximity of turbulence generation devices (fence, roughness) by the snappyHexMesh toolbox. The total grid number is approximately 9.1 million. Moreover, the boundary conditions for the numerical simulation are similar to those of the physical

Table 2
Summary of the numerical schemes.

Turbulence model	LES
SGS model	standard Smagorinsky ($C_s = 0.1$)
Time discretization scheme	2nd order implicit backward scheme
Space discretization scheme	Convective term: 2nd order LUST scheme (in momentum equations), 2nd order limited linear scheme (in the energy equation) Diffusion term: 2nd order Gauss linear corrected
Linear equation solvers	Velocity and temperature: PBiCGStab Pressure: GAMG
Time step size	0.001 s
Max CFL number	< 1
Sampling duration	30 s
Decoupling method	PIMPLE
Software	OpenFOAM-v2012

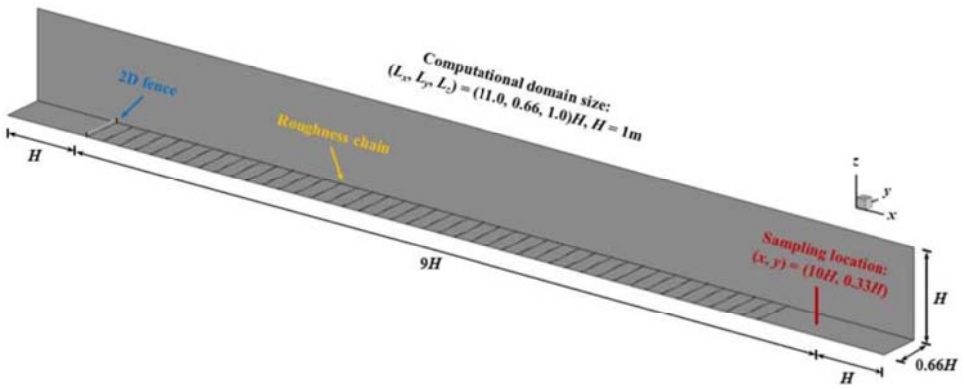

Fig. 3. Configuration of the numerical wind tunnel for stably-stratified turbulent flows over flat terrain.

Table 3
Boundary conditions for modeling stably-stratified ABL flows over flat terrain by LES.

Locations	Boundary conditions
Inlet	Dirichlet condition for velocity and temperature: $u = U_\infty = 1.57$ m/s, $v = w = 0$ $\theta(K) = \begin{cases} 285.15 + 100\,z & z < 0.6H \\ 345.15 + 33(z - 0.6) & 0.6H \le z < 1.0H \end{cases}$ $(H = 1\text{m})$ Neumann condition for pressure: $\partial p/\partial n = 0$
Outlet	Dirichlet condition for p; Neumann condition for u, v, w, θ
Spanwise sides	Symmetric condition
Top	Free slip condition for u, v, w; Neumann condition for p, θ
Bottom	No-slip condition for u, v, w; Neumann condition for p; Dirichlet condition for θ: $\theta_s = 282.15$ K

wind tunnel, as summarized in Table 3. The space and time discretization schemes employed in the numerical model are identical to those in Section 2.4. The time increment is set as 0.001 s and a sampling duration of 30 s is employed for the following analysis of turbulent statistics after the initial transient effects at the first 10 s disappear. The velocity and temperature profiles are evaluated at a downstream distance of 9 H from the 2D fence, where the boundary layer is fully developed.

The vertical distributions of mean velocity, mean temperature and turbulence fluctuation for the SBL over flat terrain are depicted in Fig. 4. To compare with previous experimental data from Ohya and Uchida [52], the freestream velocity U_∞ and the temperature difference $\Delta\theta = \theta_\infty - \theta_s$, where θ_∞ is the ambient air temperature at the boundary layer height δ of 0.45 m, are chosen to normalize the velocity and temperature, respectively. On the whole, both the mean and fluctuating streamwise velocity of the SBL obtained from the laboratory experiment can be reasonably reproduced by the present LES simulation, as shown in Fig. 4(a) and Fig. 4(c). Additionally, it is demonstrated from Fig. 4(b) that the mean temperature increases nearly linearly with height, which is also favorably captured by the LES turbulence model. It should be mentioned that this type of SBL has been frequently reported based on many full-scale observations, which exhibits stronger wind shear compared to the neutral ABL [16,36,51,62,70].

3.2. ABL flows over flat terrain under unstable stratification

For the numerical modelling of the ABL flow under unstable stratification using the LES turbulence model, a pre-designed temperature profile is imposed on the upstream boundary and the ground temperature is set to 70 °C, which are similar to the wind tunnel test performed by Ohya and Uchida [53]. The computational domain size is 9 H (length) × H (width) × H (height) in Fig. 5. With respect to the mesh system, a background mesh with a uniform horizontal grid size of 0.01 H is first constructed by blockMesh and then refined by using the snappyHexMesh toolbox near the turbulence generation device. The total mesh quantity is about 8.9 million. Additionally, the boundary conditions applied in the numerical simulation are almost consistent with those of the laboratory experiment, as listed in Table 4. Moreover, the numerical schemes are the same as those in Section 2.4. The time step size is specified as 0.001 s. The first 10 s is employed to spin up the transient flow field, and the following 30 s is subsequently used for the data analysis. The velocity and temperature profiles are evaluated at a downstream position of 7H from the 2D block, where the fully-developed boundary layer is generated.

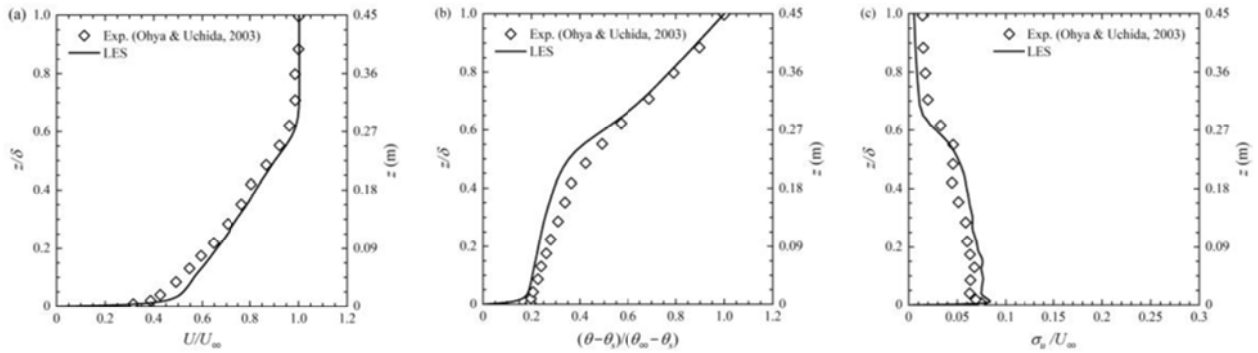

Fig. 4. Vertical profiles of physical flow variables for stably-stratified ABL flows over flat terrain: (a) mean streamwise velocity, (b) mean temperature, (c) streamwise turbulence fluctuation.

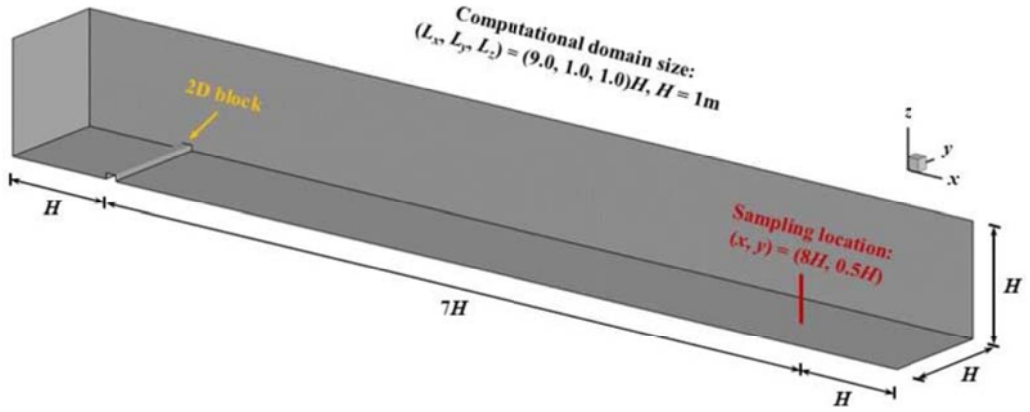

Fig. 5. Configuration of the numerical wind tunnel for unstably-stratified turbulent flows over flat terrain.

Table 4
Boundary conditions for modeling unstably-stratified turbulent flows over flat terrain by LES simulations.

Locations	Boundary conditions
Inlet	Dirichlet condition for velocity and temperature: $u = U_\infty = 1.5\ \mathrm{m/s},\ v = w = 0$ $\theta(K) = \begin{cases} 288.15 & z < 0.21H \\ 288.15 + 500(z - 0.21) & 0.21H \le z < 0.33H \\ 348.15 + 33(z - 0.33) & 0.33H \le z < 1.00H \end{cases}$ $(H = 1\mathrm{m})$ Neumann condition for pressure: $\partial p/\partial n = 0$
Outlet	Dirichlet condition for p; Neumann condition for $u,\ v,\ w,\ \theta$
Spanwise sides	Symmetric condition
Top	Free slip wall condition for $u,\ v,\ w$; Neumann condition for $p,\ \theta$
Bottom	No-slip condition for $u,\ v,\ w$; Neumann condition for p; Dirichlet condition for θ: $\theta_s = 343.15$ K

The vertical distributions of mean velocity and temperature for the convective boundary layer (CBL) over flat terrain are presented in Fig. 6 (a) and Fig. 6(b), respectively. It is observed that the simulated results are in good agreement with the experimental data. The constant values of mean velocity and temperature are found in the range of $z/z_i = 0.2 - 0.8$ as a result of vigorous convective mixing, where z_i is the inversion height and is equal to 0.28 m. In the upper part of the mean temperature profile, the pronounced temperature gradient characteristic of a strong inversion layer is accurately captured by LES. In addition, the longitudinal turbulence fluctuation predicted by the LES simulation aligns well with the experiments as shown in Fig. 6(c). The CBL exhibits weaker wind shear compared to the NBL.

3.3. Turbulent flows over steep hill under neutral stratification

The performance of numerical models in simulating turbulent flows over steep hill is subsequently validated using the wind tunnel tests carried out by Ishihara and Hibi (1999). It should be noted that the hill shape, hill slope and surface roughness in this validation study are adopted in the following simulations to clarify the effects of thermal stratification on turbulent flow fields over hilly terrain.

For the LES simulation, the computational setups are kept almost the same as those in Sections 2.2-2.4. In terms of the RANS simulations, the numerical domain and grid system as well as discretization schemes are specified as shown in Ishihara and Hibi [26]. It should be noted that the k-ε turbulence model is among the most popular RANS models for the wind energy industry. Therefore, the k-ε turbulence model is employed herein for comparison purposes. Fig. 7 presents the vertical distributions of mean velocity and turbulence fluctuation for turbulent flows over a 3-D steep hill predicted by RANS and LES models. To validate against the experimental data, the hill height h and the freestream velocity U_∞ are used for the normalization. On the upwind side of the hill, the vertical profiles of mean velocity and turbulence fluctuation can be reasonably reproduced by both RANS and LES. However, the RANS model is insufficient to accurately capture the flow separation induced by the strong unfavorable pressure gradient on the downwind side, as illustrated in Fig. 7(a). In addition, the turbulence fluctuation in the wake region is significantly underestimated by RANS simulations, as depicted in Fig. 7(b). In contrast, both the mean flow and turbulence characteristics behind the hill are well predicted by the LES simulation.

4. Results and discussion

The effects of thermal stratification on turbulent flow fields over a typical hilly terrain are comprehensively discussed in this section. The characteristics of approaching thermally-stratified ABL flows are first presented and compared with the stability-dependent wind speed profiles in Section 4.1. The flow patterns near a steep hill are then investigated under different thermal stability conditions in Section 4.2. The mean flow and turbulence characteristics around a steep hill are examined and evaluated by a simple formula considering the topographic effect and thermal stratification in Section 4.3. Finally, the force-balance analysis is conducted to clarify the mechanism of flow phenomena for thermally-stratified boundary layers over hilly terrain in Section 4.4.

4.1. Characteristics of approaching flows

Fig. 8 shows the vertical distributions of mean velocity and turbulence fluctuation for approaching ABL flows under different thermal stratification. The hill height h and the freestream velocity U_∞ are employed for the normalization. The mean velocity shows a significant decrease in the proximity of ground surface. Additionally, the largest velocity gradient is observed under stable stratification, implying the occurrence of the strongest vertical wind shear. In contrast, the mean velocity is almost kept constant in a certain range of $z/h = 1 - 4$ under unstable stratification due to the presence of vigorous vertical turbulent mixing. Moreover, it is exhibited that the turbulence intensity is enhanced by the unstable stratification, while they are suppressed by the stable stratification.

To quantify the influence of thermal stratification, the Monin–Obukhov length scale (L) is adopted in this study. Accordingly, the mean velocity profile under different atmospheric stability conditions can be described as follows:

$$u(z) = \frac{u_*}{\kappa}\left[ln\left(\frac{z}{z_0}\right) - \psi\left(\frac{z}{L}\right)\right] \tag{9}$$

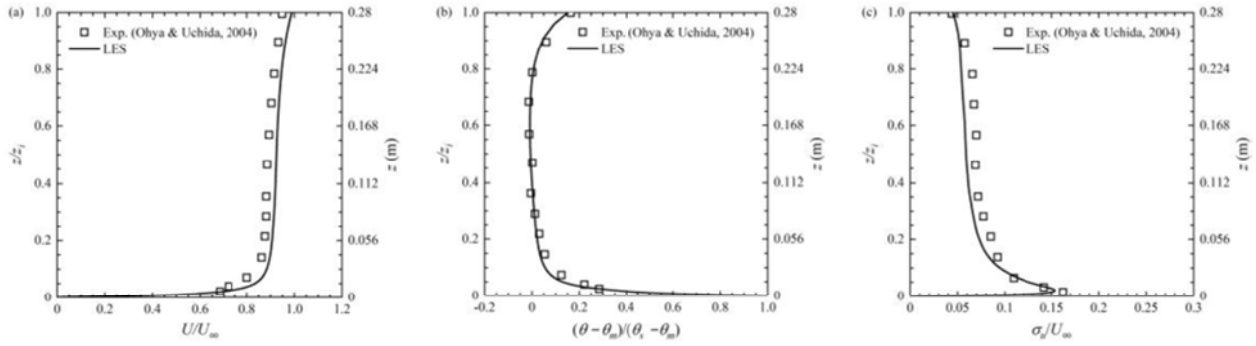

Fig. 6. Vertical profiles of physical flow variables for unstably-stratified ABL flows over flat terrain: (a) mean streamwise velocity, (b) mean temperature, (c) streamwise turbulence fluctuation.

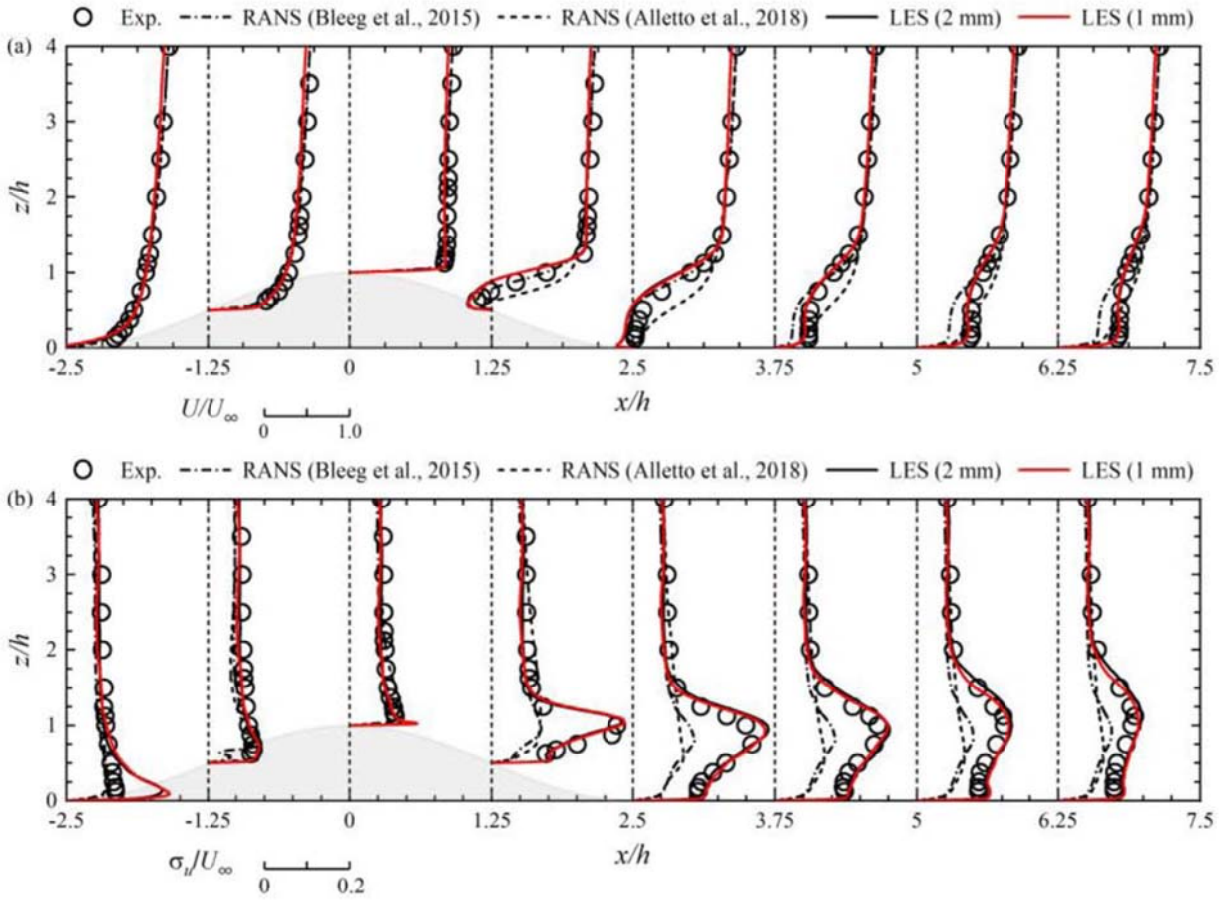

Fig. 7. Vertical profiles of physical flow variables for neutrally-stratified ABL flows over a steep hill: (a) mean velocity and (b) turbulence fluctuation in the streamwise direction.

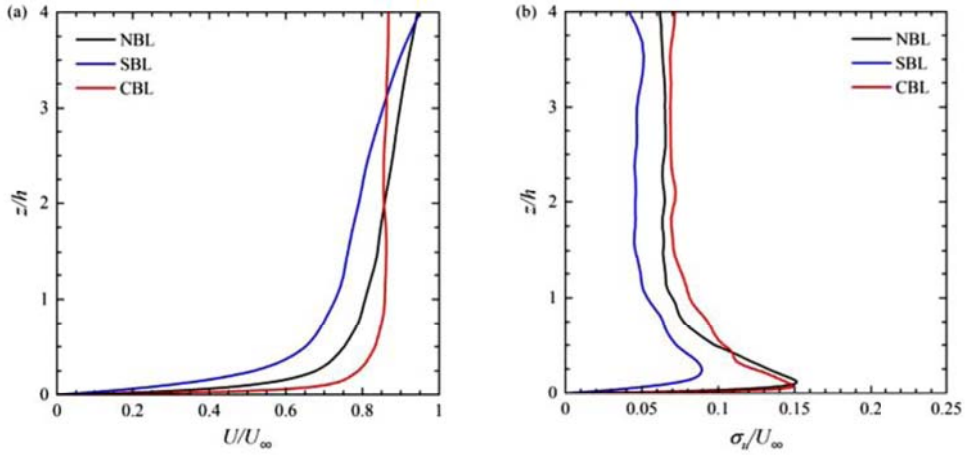

Fig. 8. Vertical profiles of physical flow variables for different approaching thermally stratified ABL flows: (a) mean velocity and (b) turbulence fluctuation.

$$\psi\left(\frac{z}{L}\right) = \begin{cases} -5\left(\frac{z}{L}\right) & L > 0 \\ 2ln\left(\frac{1+x}{2}\right) + ln\left(\frac{1+x^2}{2}\right) - 2tan^{-1}x + \frac{\pi}{2} & L < 0 \\ x = [1 - 16z/L]^{1/4} & \end{cases} \tag{10}$$

where u_* is the friction velocity, κ is the von Karman constant, z_0 is the surface roughness and L is the Monin-Obukhov length scale.

Based on the classification for atmospheric stability [61], the simulated cases can further be categorized into the neutral, stable, and unstable conditions, respectively. The L is 0.30 m for the case of stable stratification and −0.05 m for the case of unstable stratification, which shows a good fit with the stability-dependent logarithmic-law wind speed profiles as depicted in Fig. 9.

4.2. Flow patterns

The time-averaged velocity contours and streamline patterns around a 3-D steep hill under different thermal stratification conditions are

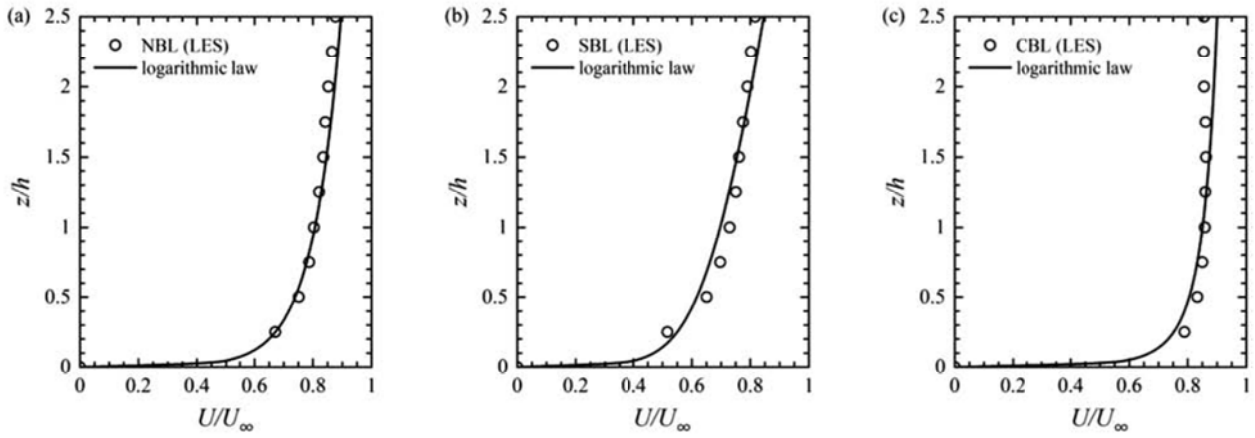

Fig. 9. Comparison of mean wind speed profiles predicted by LES and the stability-dependent logarithmic-law model under different thermal stratification: (a) neutral, (b) stable and (c) unstable.

presented in Fig. 10. It is demonstrated that the symmetrical twin-vortices are formed behind the hill crest regardless of atmospheric stability conditions. However, comparing with the case of neutral stratification, the extent of the reversal flow zone on the lee side of a hill exhibits a marginal increase under stable stratification, while it is reduced under unstable stratification. Moreover, as the thermal instability intensifies, it is found that the mean horizontal streamlines converge towards the wake centerline faster under the unstable stratification.

Fig. 11 displays the mean velocity contours and streamline distributions around a 3-D steep hill under different thermal stratification conditions. It is found that the separation bubble under unstable stratification is smaller than that under neutral and stable stratification. Furthermore, the time-averaged streamlines present a distinct upward deflection under unstable stratification, which is attributed to the enhanced vertical fluid motions induced by the strong positive buoyancy force. Conversely, in the stable case, the airflow rising upstream of the hill is prevented from rising downstream of the hill by negative buoyancy effects.

In addition to the mean flow patterns, it is also interesting to visualize the impacts of atmospheric stratification on the instantaneous flow structures around typical hilly terrain. The evolution of unsteady vortices downstream of a 3-D steep hill are displayed on the vertical slice crossing the hill center as shown in Fig. 12. The wake development downstream of the hill is closely correlated with the thermal stability of the approaching flows. The separated vortices are intensified and lifted in the CBL case. On the other hand, for the SBL case, the vortices behind the 3-D steep hill are damped and are confined within a limited altitude.

4.3. Statistical characteristics

With the aim of quantifying the impacts of thermal stratification on flow fields over topography, the profiles of mean velocity and turbulence fluctuation over a 3-D steep hill under various atmospheric stability conditions are presented in Fig. 13. The experimental data of neutrally stratified ABL flow over a 3-D steep hill by Ishihara et al. [27] are superimposed on the figure. Overall, the turbulent statistics predicted by LES align well with the experimental data under neutral stratification. As revealed in Fig. 13(a), the prominent flow acceleration is revealed at the hilltop and the recirculation zone is identified at the lee slope. In general, the vertical distributions of mean velocity over hilly terrain are strongly affected by thermal stratification. In comparison with the neutral condition, the near-surface wind speed is increased in the unstable condition, while it is reduced in stable condition. Moreover, it can be observed from Fig. 13(b) that the turbulence fluctuation is amplified by unstable stratification but damped by stable stratification. Under unstable conditions, the convective motions are enhanced and turbulence generation and mixing amplified.

To explain the influence of thermal stratification on airflow characteristics over steep hilly topography, the following analysis endeavors to shed light on the mechanisms governing the mean flow field around a steep 3-D hill under thermal stratification. The effects of topography and atmospheric stability are assumed to be separated for predicting the mean wind speed over complex terrain. Firstly, the terrain correction factor $C_U^{terrain}(x,y,z')$ is calculated based on the CFD modelling of ABL flows over hills under neutral stratification, where z' denotes the height from the ground of z_s as shown in Eq. (8). Secondly, the stability correction factor $C_U^{stability}(z')$ is derived using the Monin–Obukhov similarity law to account for the influence of thermal stratification on mean wind speed profiles over flat terrain. Finally, the combined effects of topography and atmospheric stability on mean wind speed can be evaluated by Eq. (11) as

$$U_{terrain}^{stratified}(x,y,z') = U_{ref}^{neutral} \times C_U^{terrain}(x,y,z') \times C_U^{stability}(z') \tag{11}$$

$$C_U^{terrain}(x,y,z') = \frac{U_{terrain}^{neutral}(x,y,z')}{U_{ref}^{neutral}} \tag{12}$$

$$C_U^{stability}(z') = \frac{\left[ln\left(\frac{z'}{z_0}\right) - \psi\left(\frac{z'}{L}\right)\right] \Big/ \left[ln\left(\frac{z'_{ref}}{z_0}\right) - \psi\left(\frac{z'_{ref}}{L}\right)\right]}{\left[ln\left(\frac{z'}{z_0}\right)\right] \Big/ \left[ln\left(\frac{z'_{ref}}{z_0}\right)\right]} \tag{13}$$

where $U_{ref}^{neutral}$ is the mean wind speed of the approaching neutrally-stratified ABL flow at $x = -5h$ and at the reference height of $z'_{ref} = 2.5h$.

The vertical distributions of terrain correction factor and stability correction factor are plotted in Fig. 14. Compared to the flat upstream terrain at $x = -5h$, it is found that the near-surface wind speed enhances significantly at the hilltop and reduces remarkably in the hill wake at $x = 2.5h$ under neutral stratification, as illustrated in Fig. 14(a). In addition, it is revealed by Monin–Obukhov similarity theory that the mean wind speed over flat terrain is increased in the unstable condition but decreased in the stable condition, as displayed in Fig. 14(b).

Fig. 15 exhibits the comparison of normalized mean wind speed profiles for thermally-stratified boundary layer flows over a steep 3-D hill predicted by the LES simulation and the analytical model as shown in Eq. (11). U_{ref} is the mean wind speed of each location at the reference height of $z_{ref} = 2.5h$. A favorable agreement is achieved between the analytical solution and numerical simulation. On the flat

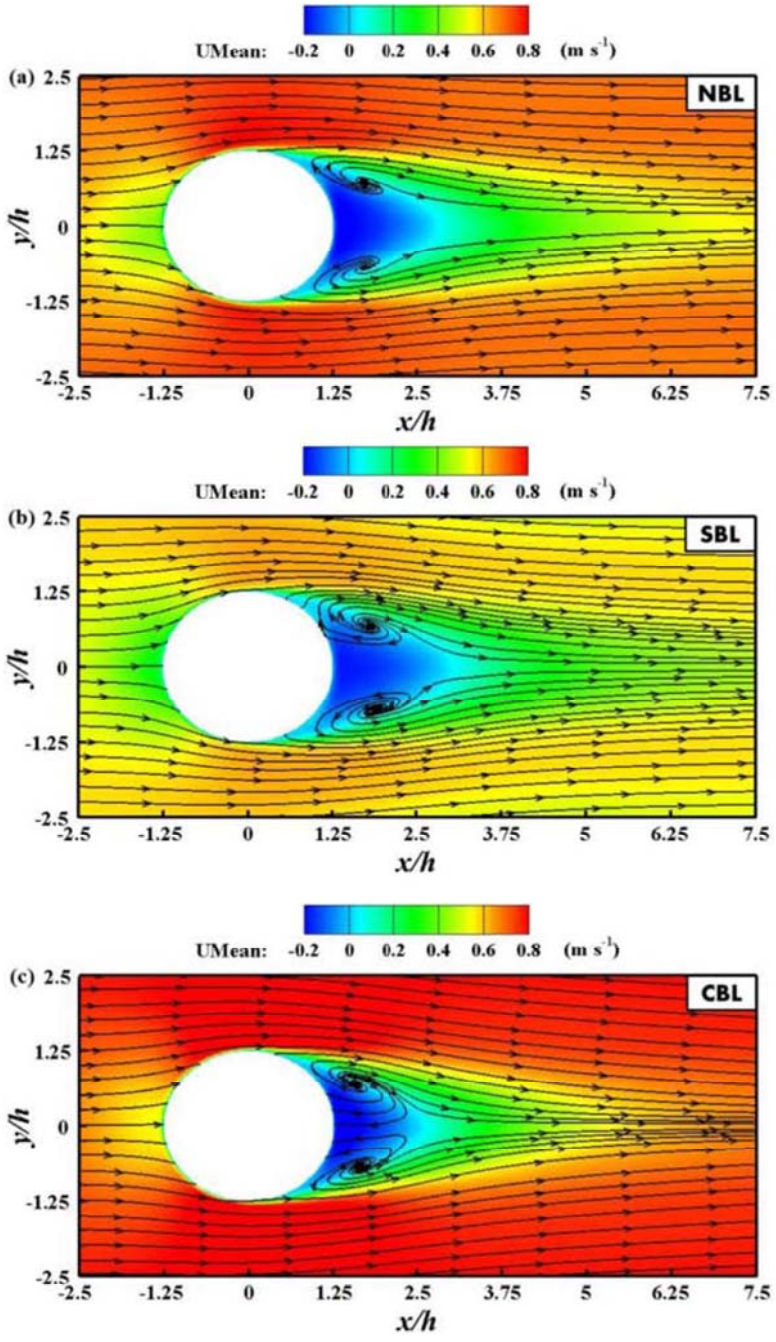

Fig. 10. Effects of thermal stratification on mean velocity contours and streamline patterns around a 3-D steep hill on the horizontal slice with a half hill height: (a) neutral, (b) stable and (c) unstable.

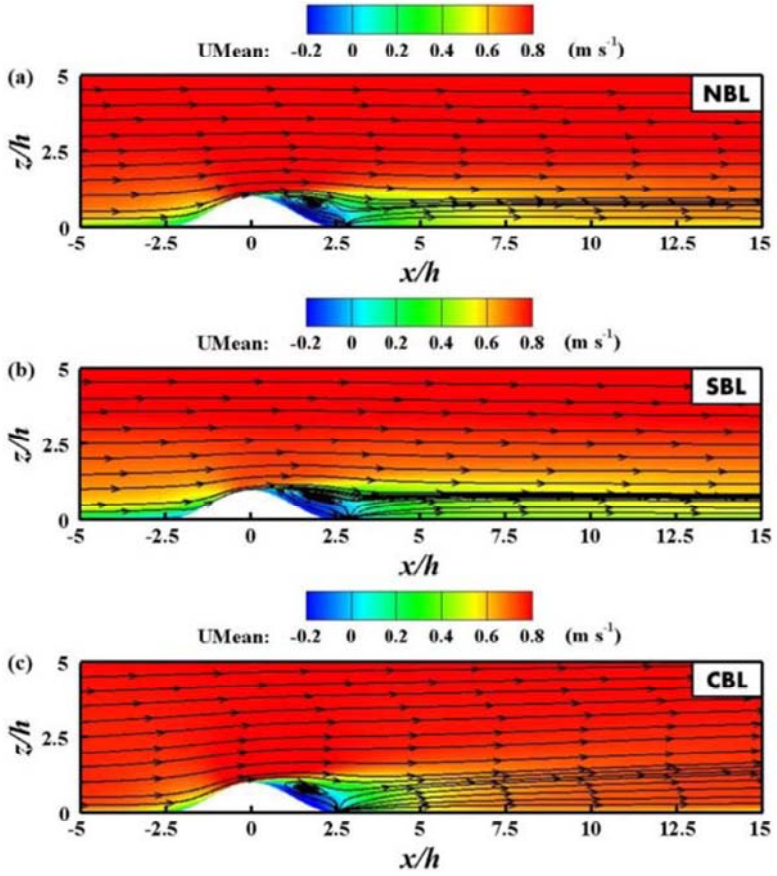

Fig. 11. Effects of thermal stratification on mean velocity contours and streamline patterns around a 3-D steep hill on the vertical slice crossing the hill center: (a) neutral, (b) stable and (c) unstable.

upstream region, the mean flow profiles in Fig. 15(a) are primarily dominated by atmospheric stability conditions and deviation of mean wind speed profiles can be attributed to the effect of thermal stratification as shown in Eq. (13). As the airflow moves upward to the hill crest, the speedups in Fig. 15(b) are determined by both topographic effect and thermal stratification. Both the terrain induced force by steep topography and the buoyancy induced force exerted by thermal stratification act as a pivotal role in accelerating the wind flow at the hilltop. However, in the near-wake region, the slight discrepancies of mean velocity profiles under different thermal stratification are observed close to ground surface in Fig. 15(c). This implies that the time-averaged characteristics of wake flow behind the hill are highly dependent on the topographic effect.

4.4. Force-balance analysis

To elucidate the impact of atmospheric stability on the formation of flow fields around hilly terrain, the vertical force balance is first examined by the time-averaged Navier–Stokes equation in the vertical direction. The vertical components of the time-averaged Navier–Stokes equation can be derived as

$$U\frac{\partial W}{\partial x}+V\frac{\partial W}{\partial y}+W\frac{\partial W}{\partial z}=-\frac{1}{\rho}\frac{\partial P}{\partial z}-\left(\frac{\partial uw}{\partial x}+\frac{\partial vw}{\partial y}+\frac{\partial ww}{\partial z}\right)+D_w \tag{14}$$

where u, v and w denote the longitudinal, lateral and vertical components of fluctuating velocity. The left-hand side consists of mean longitudinal (A_{xw}), lateral (A_{yw}) and vertical (A_{zw}) advection terms. The right-hand side is constituted by the vertical pressure gradient term (P_z), turbulent force term (T_w) and diffusion term (D_w). The buoyancy effects are incorporated into the pressure gradient terms for both stable and unstable cases. The vertical force balances at the hilltop under different thermal stratification are shown in Fig. 16(a-c). The longitudinal advection term is almost balanced with the vertical pressure gradient term, while the contributions from the other terms are negligible. In addition, the increasing vertical pressure gradient enhances the vertical momentum transport under unstable stratification. Furthermore, the magnitude of the vertical pressure gradient reduces with height. In contrast to the hilltop, the vertical force balance in the wake region becomes much more complicated due to the presence of terrain-induced turbulence, as illustrated in Fig. 16(d-F). The vertical pressure gradient term and the turbulent force term are dominant near the ground, and almost cancel each other out. However, at the higher elevation, the streamwise advection term (A_{xw}) shows contributions to the vertical force balance, particularly in the unstable case. Compared with the neutral and stable stratification cases, the positive longitudinal advection term is observed at a certain height under unstable stratification, implying the vertical transport of momentum driven by the upward flow.

The mechanism of mean wind speed variation along the central axis of curved topography in the longitudinal direction is further clarified by considering the force balance of longitudinal components of the time-

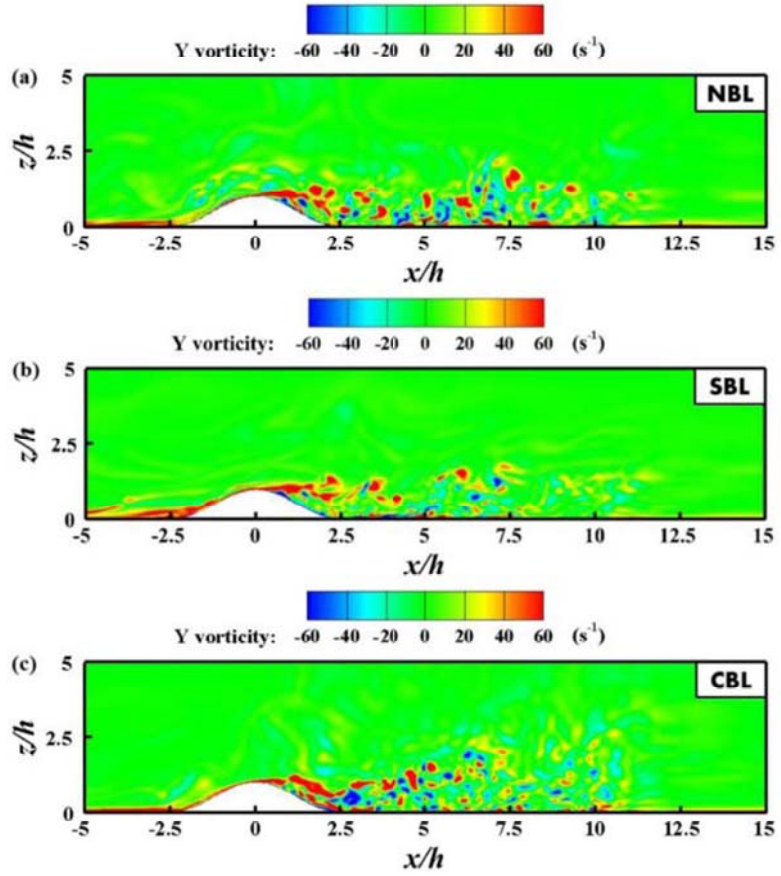

Fig. 12. Effects of thermal stratification on instantaneous vortices around a 3-D steep hill on the vertical slice crossing the hill center: (a) neutral, (b) stable and (c) unstable.

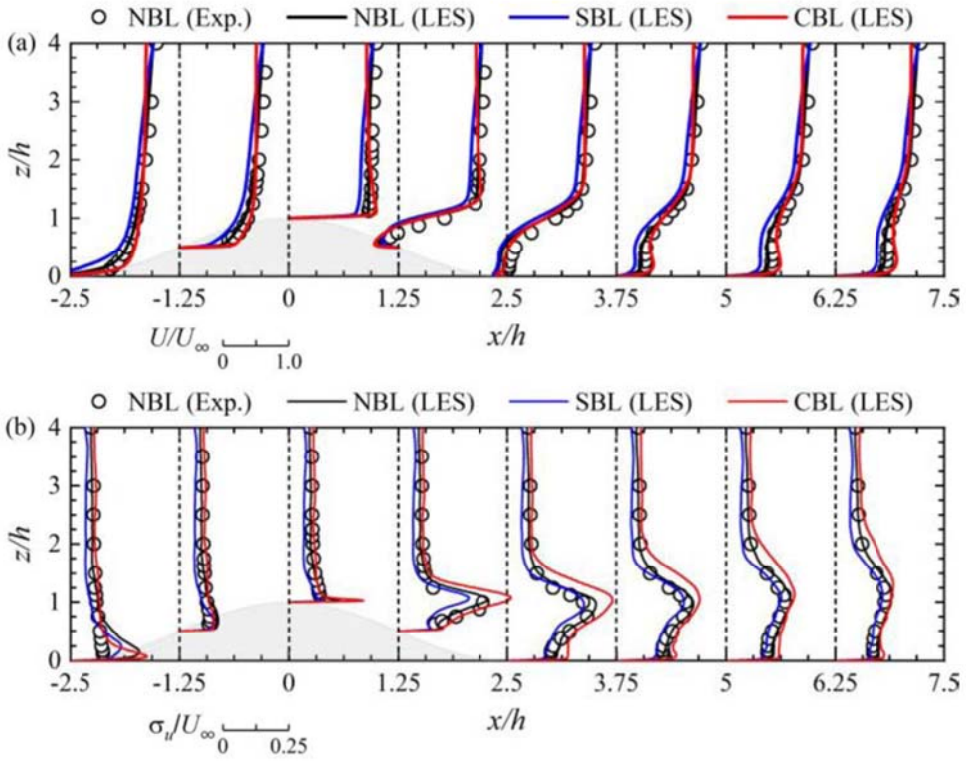

Fig. 13. Profiles of (a) mean velocity and (b) turbulence fluctuation around a 3-D steep hill under different thermal stratification.

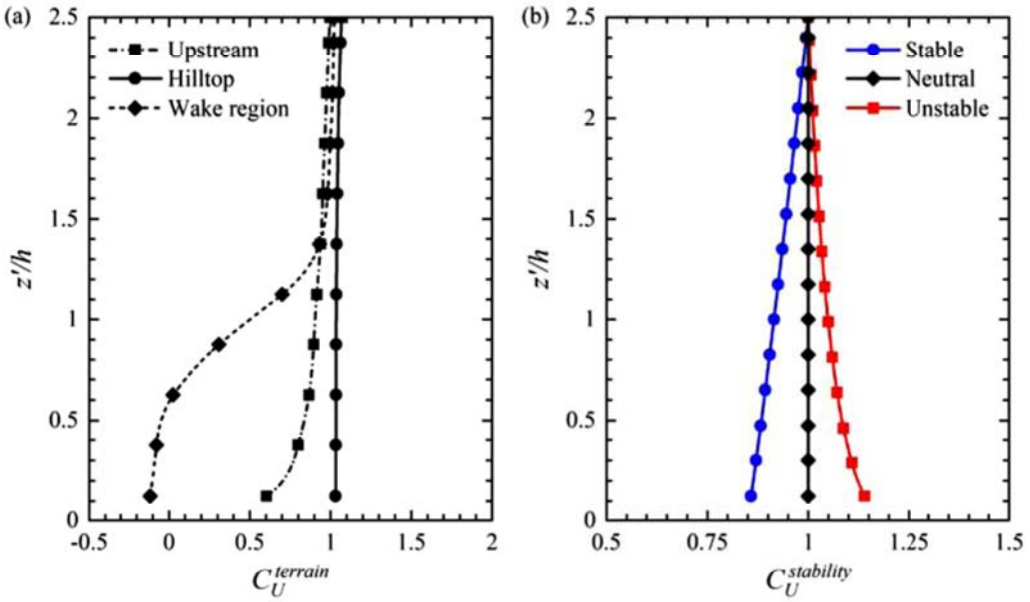

Fig. 14. Vertical distributions of (a) terrain correction factor for mean wind speed over a 3-D steep hill and (b) stability correction factor for mean wind speed over flat terrain.

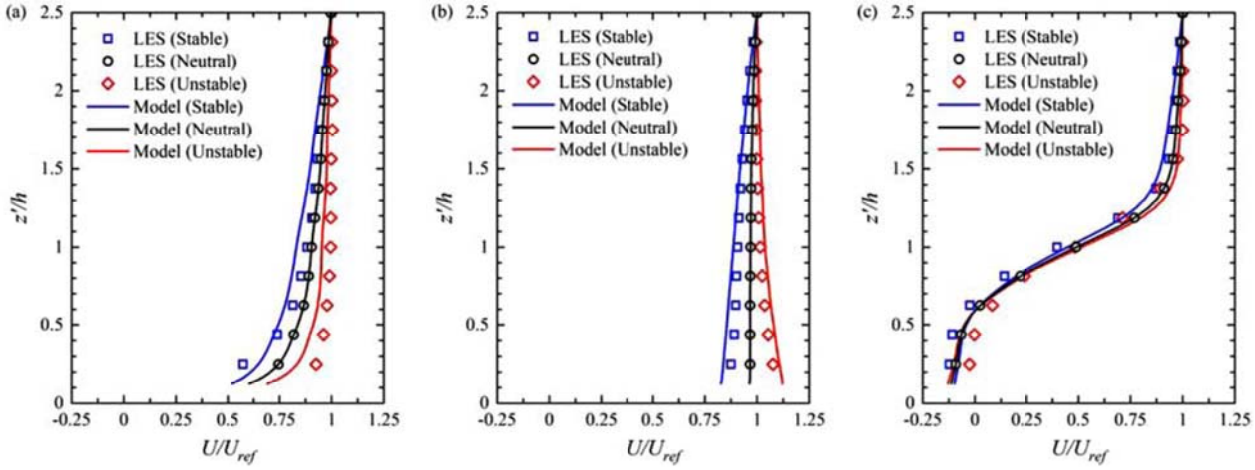

Fig. 15. Comparison of mean wind speed profiles over a 3-D steep hill under different thermal stratification: (a) upstream region ($x = -5h$), (b) hilltop ($x = 0$) and (c) wake region ($x = 2.5h$).

averaged Navier–Stokes equation, which can be formulated as

$$U\frac{\partial U}{\partial x} + V\frac{\partial V}{\partial y} + W\frac{\partial U}{\partial z} = -\frac{1}{\rho}\frac{\partial P}{\partial x} - \left(\frac{\partial uu}{\partial x} + \frac{\partial uv}{\partial y} + \frac{\partial uw}{\partial z}\right) + D_u \tag{15}$$

The first and second terms to the left of the equal sign refer to longitudinal (A_{xu}), lateral (A_{yu}) and vertical (A_{zu}) advection terms, respectively. The right side of the formula includes the longitudinal pressure gradient term (P_x), turbulent force term (T_u) and diffusion term (D_u).

Fig. 17 shows the longitudinal force balance for different thermally-stratified ABL flows over a 3-D steep hill on the central plane at $y = 0$. At the windward region of the 3-D hill, the longitudinal pressure gradient term is approximately canceled by the longitudinal advection term. As a consequence of the favorable pressure gradient ($\partial P/\partial x < 0$) caused by the hill, the airflow accelerates on the upstream slope and the maximum speed-up occurs at the hill summit. However, in addition to the longitudinal pressure gradient term and the longitudinal advection term, both the vertical advection term and the turbulent force term make contributions to the longitudinal force balance in the hill wake are illustrated in Fig. 17(a-c). Therefore, the prediction accuracy of mean flow fields in the wake region is considerably influenced by the prediction accuracy of the wake turbulence. This can be used to explain why the RANS models are incapable of accurately predicting the mean wind speed distributions in the wake of steep topography. Moreover, the adverse pressure gradient ($\partial P/\partial x > 0$) is observed behind the hill, leading to flow separation and deceleration. Furthermore, it is observed that the magnitude of the streamwise pressure gradient and the turbulent force term decreases with increasing altitude as illustrated in Fig. 17 (d-F). Correspondingly, the variations of mean streamwise velocity are smaller at higher locations as shown in Fig. 13(a).

5. Conclusions

In this study, LES simulations are carried out to clarify the influence of thermal stratification on turbulent flow fields over a 3-D steep hill.

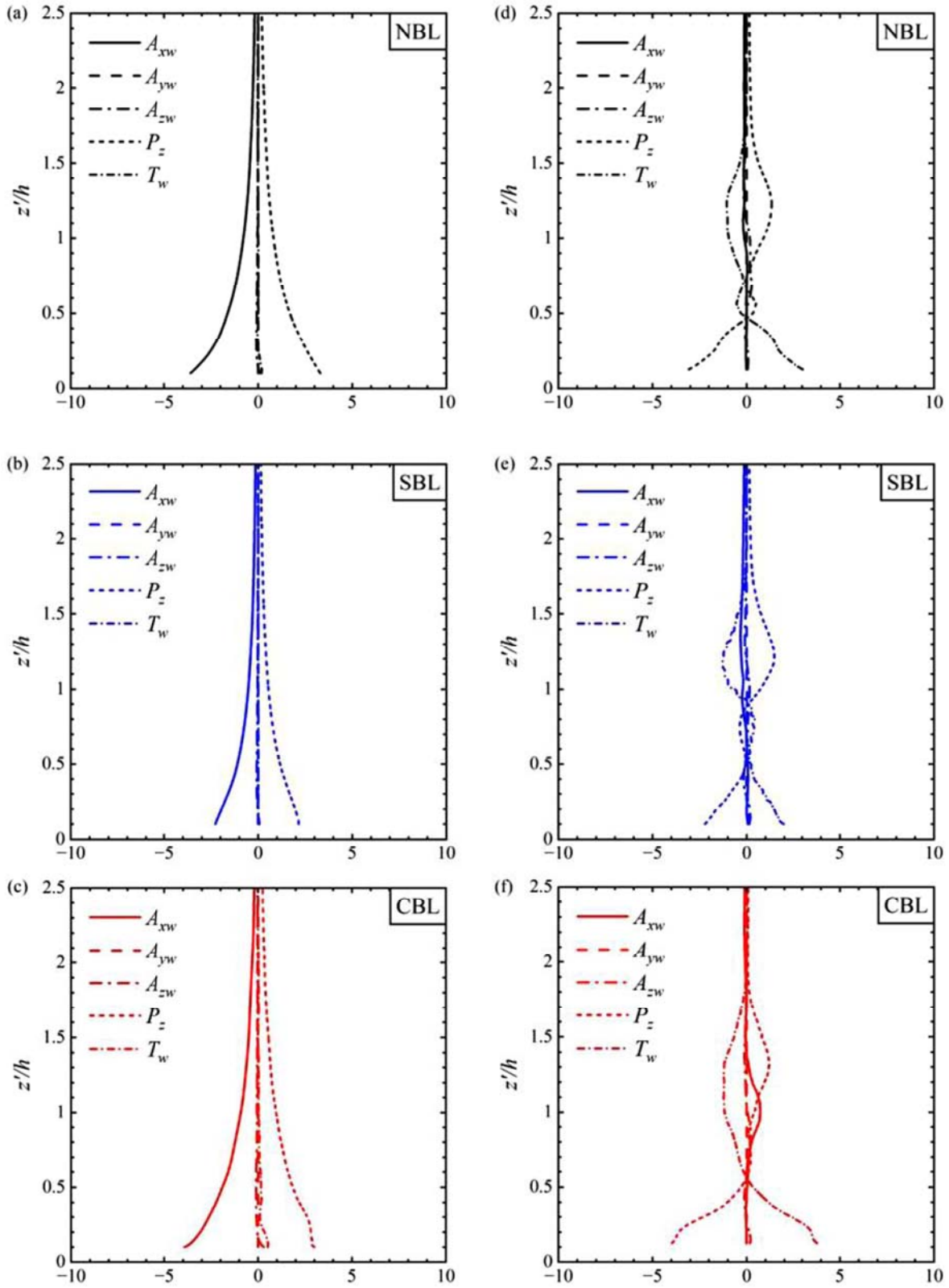

Fig. 16. Vertical distributions of normalized vertical force terms of Navier–Stokes equation at typical locations under different thermal stratification: (a) neutral, (b) stable and (c) unstable at $x = 0$; (d) neutral, (e) stable and (f) unstable at $x = 2.5h$.

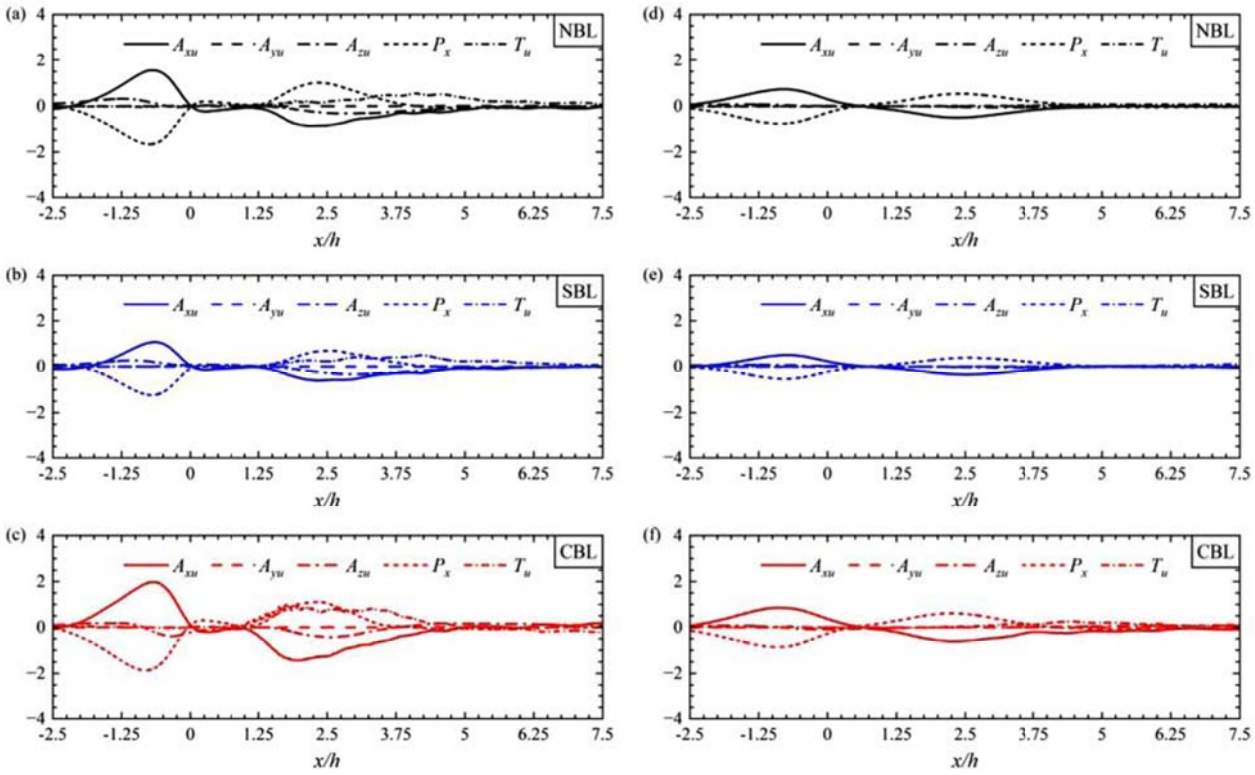

Fig. 17. Longitudinal distributions of normalized longitudinal force terms of Navier–Stokes equation at different elevations under different thermal stratification: (a) neutral, (b) stable and (c) unstable at $z = 1.5h$; (d) neutral, (e) stable and (f) unstable at $z = 2h$.

The accuracy of numerical model is validated by comparing predicted thermally-stratified atmospheric boundary layer (ABL) flows over flat and hilly terrain with experimental data from wind tunnel tests. Both flow patterns and turbulent statistics around the steep hilly terrain are elucidated under various atmospheric stability conditions. The effects of topography and thermal stratification on the mean flow fields over hilly terrain are analyzed. Furthermore, the mechanisms governing the formation of flow fields over topography under different thermal stability conditions are explored based on force balance analysis. The principal conclusions of the present study are briefly summarized as follows:

1. The LES turbulence model provides accurate prediction of stable and unstable boundary layer flows over flat terrain as well as turbulent flows over steep hilly terrain, since it can successfully capture both topography and thermally induced turbulence structures.
2. The mean velocities and turbulence fluctuations over a 3-D steep hill are enhanced under unstable stratification and reduced under stable stratification. The thermal stratification is a dominant factor in characterizing the upstream flow fields, while the near-wake flow fields are primarily influenced by topographic conditions. Moreover, the flow characteristics at the hilltop are affected by both topography and thermal stratification.
3. The vertical and longitudinal force balances on the downwind side of the hill differ significantly from those on the upwind side. Both the vertical and longitudinal force balances with the mean longitudinal advection term and the pressure gradient term on the upstream side of the hill, while the turbulent force term plays a significant role in the vertical and longitudinal force balances in the hill wake.

CRediT authorship contribution statement

Tong Zhou: Writing – original draft, Visualization, Software, Investigation, Formal analysis, Data curation. **Takeshi Ishihara:** Writing – review & editing, Validation, Supervision, Resources, Methodology, Conceptualization.

Declaration of competing interest

The authors declare that they have no known competing financial interests or personal relationships that could have appeared to influence the work reported in this paper.

Acknowledgment

This research is carried out as part of a joint program for next generation energy infrastructure with Toshiba Energy Systems & Solutions Corporation, J-POWER, Shimizu Corporation, Class NK, Tokyo Gas, CHOBU Electric Power. The authors express their deepest gratitude to the concerned parties for their assistance during this study. The authors also wish to thank the China Scholarship Council (Grant No. CSC202107090014) for the funding support.

Data availability

Data will be made available on request.

References

[1] Abd Razak A, Hagishima A, Ikegaya N, Tanimoto J. Analysis of airflow over building arrays for assessment of urban wind environment. Build Environ 2013;59:56–65. https://doi.org/10.1016/j.buildenv.2012.08.007.
[2] Abkar M, Sharifi A, Porté-Agel F. Wake flow in a wind farm during a diurnal cycle. J Turbul 2016;17(4):420–41. https://doi.org/10.1080/14685248.2015.1127379.
[3] Alletto M, Radi A, Adib J, Langner J, Peralta C, Altmikus A, Letzel M. E-Wind: steady state CFD approach for stratified flows used for site assessment at Encrcon. J Phys Conf Ser 2018;7:072020. https://doi.org/10.1088/1742-6596/1037/7/072020.
[4] Athanassiadou M, Castro IP. Neutral flow over a series of rough hills: a laboratory experiment. Boundary-Layer Meteorol 2001;101:1–30. https://doi.org/10.1023/A:1019250801054.

[5] Bleeg J, Digraskar D, Woodcock J, Corbett JF. Modeling stable thermal stratification and its impact on wind flow over topography. Wind Energy 2015;18 (2):369–83. https://doi.org/10.1002/we.1692.

[6] Blocken B, van der Hout A, Dekker J, Weiler O. CFD simulation of wind flow over natural complex terrain: case study with validation by field measurements for Ria de Ferrol, Galicia, Spain. J Wind Eng Ind Aerod 2015;147:43–57. https://doi.org/10.1016/j.jweia.2015.09.007.

[7] Bradley S, Perrott Y, Behrens P, Oldroyd A. Corrections for wind-speed errors from sodar and lidar in complex terrain. Boundary-Layer Meteorol 2012;143:37–48. https://doi.org/10.1007/s10546-012-9702-0.

[8] Bradley S, von Hünerbein S, Mikkelsen T. A bistatic sodar for precision wind profiling in complex terrain. J Atmos Ocean Technol 2012;29(8):1052–61. https://doi.org/10.1175/JTECH-D-11-00035.1.

[9] Britter RE, Hunt JCR, Richards KJ. Air flow over a two-dimensional hill: studies of velocity speed-up, roughness effects and turbulence. Q J R Meteorol Soc 1981;107 (451):91–110. https://doi.org/10.1002/qj.49710745106.

[10] Cao S, Tamura T. Experimental study on roughness effects on turbulent boundary layer flow over a two-dimensional steep hill. J Wind Eng Ind Aerod 2006;94(1): 1–19. https://doi.org/10.1016/j.jweia.2005.10.001.

[11] Cao S, Tamura T. Effects of roughness blocks on atmospheric boundary layer flow over a two-dimensional low hill with/without sudden roughness change. J Wind Eng Ind Aerod 2007;95(8):679–95. https://doi.org/10.1016/j.jweia.2007.01.002.

[12] Cao S, Wang T, Ge Y, Tamura Y. Numerical study on turbulent boundary layers over two-dimensional hills—Effects of surface roughness and slope. J Wind Eng Ind Aerod 2012;104:342–9. https://doi.org/10.1016/j.jweia.2012.02.022.

[13] Carpenter P, Locke N. Investigation of wind speeds over multiple two-dimensional hills. J Wind Eng Ind Aerod 1999;83(1–3):109–20. https://doi.org/10.1016/S0167-6105(99)00065-3.

[14] Chaudhari A, Vuorinen V, Hämäläinen J, Hellsten A. Large-eddy simulations for hill terrains: validation with wind-tunnel and field measurements. Comput Appl Math 2018;37:2017–38. https://doi.org/10.1007/s40314-017-0435-z.

[15] Conan B, Chaudhari A, Aubrun S, van Beeck J, Hämäläinen J, Hellsten A. Experimental and numerical modelling of flow over complex terrain: the Bolund hill. Boundary-Layer Meteorol 2016;158:183–208. https://doi.org/10.1007/s10546-015-0082-0.

[16] Derbyshire SH. Stable boundary layers: observations, models and variability part I: modelling and measurements. Boundary-Layer Meteorol 1995;74(1–2):19–54. https://doi.org/10.1007/BF00715709.

[17] Dhamankar NS, Blaisdell GA, Lyrintzis AS. Overview of turbulent inflow boundary conditions for large-eddy simulations. AIAA J 2018;56(4):1317–34. https://doi.org/10.2514/1.J055528.

[18] Diebold M, Higgins C, Fang J, Bechmann A, Parlange MB. Flow over hills: a large-eddy simulation of the Bolund case. Boundary-Layer Meteorol 2013;148:177–94. https://doi.org/10.1007/s10546-013-9807-0.

[19] Dupont S, Brunet Y, Finnigan JJ. Large-eddy simulation of turbulent flow over a forested hill: validation and coherent structure identification. Q J R Meteorol Soc 2008;134(636):1911–29. https://doi.org/10.1002/qj.328.

[20] Ferreira AD, Lopes AMG, Viegas DX, Sousa ACM. Experimental and numerical simulation of flow around two-dimensional hills. J Wind Eng Ind Aerod 1995;54: 173–81. https://doi.org/10.1016/0167-6105(94)00040-K.

[21] Flay RG, King AB, Revell M, Carpenter P, Turner R, Cenek P, Pirooz AAS. Wind speed measurements and predictions over Belmont hill, Wellington, New Zealand. J Wind Eng Ind Aerod 2019;195:104018. https://doi.org/10.1016/j.jweia.2019.104018.

[22] Gong W, Ibbetson A. A wind tunnel study of turbulent flow over model hills. Boundary-Layer Meteorol 1989;49:113–48. https://doi.org/10.1007/BF00116408.

[23] Griffiths AD, Middleton JH. Simulations of separated flow over two-dimensional hills. J Wind Eng Ind Aerod 2010;98(3):155–60. https://doi.org/10.1016/j.jweia.2009.10.011.

[24] Han Y, Stoellinger MK. RANS simulations of neutral atmospheric boundary layer flow over complex terrain with comparisons to field measurements. Wind Energy 2020;23:91–119. https://doi.org/10.1002/we.2412.

[25] Ishihara T, Fujino Y, Hibi K. A wind tunnel study of separated flow over a two-dimensional ridge and a circular hill. J Wind Eng 2001;89:573–6.

[26] Ishihara T, Hibi K. Numerical study of turbulent wake flow behind a three-dimensional steep hill. Wind Struct 2002;5:317–28. https://doi.org/10.12989/was.2002.5.2_4.317.

[27] Ishihara T, Hibi K, Oikawa S. A wind tunnel study of turbulent flow over a three-dimensional steep hill. J Wind Eng Ind Aerod 1999;83(1–3):95–107. https://doi.org/10.1016/S0167-6105(99)00064-1.

[28] Ishihara T, Qi Y. Numerical study of turbulent flow fields over steep terrain by using modified delayed detached-eddy simulations. Boundary-Layer Meteorol 2019;170(1):45–68. https://doi.org/10.1007/s10546-018-0389-8.

[29] Kamada Y, Maeda T, Yamada K. Wind tunnel experimental investigation of flow field around two-dimensional single hill models. Renew Energy 2019;136: 1107–18. https://doi.org/10.1016/j.renene.2018.09.083.

[30] Kim D, Kim T, Oh G, Huh J, Ko K. A comparison of ground-based LiDAR and met mast wind measurements for wind resource assessment over various terrain conditions. J Wind Eng Ind Aerod 2016;158:109–21. https://doi.org/10.1016/j.jweia.2016.09.011.

[31] Kim HG, Lee CM, Lim HC, Kyong NH. An experimental and numerical study on the flow over two-dimensional hills. J Wind Eng Ind Aerod 1997;66(1):17–33. https://doi.org/10.1016/S0167-6105(97)00007-X.

[32] Kobayashi MH, Pereira JCF, Siqueira MBB. Numerical study of the turbulent flow over and in a model forest on a 2D hill. J Wind Eng Ind Aerod 1994;53(3):357–74. https://doi.org/10.1016/0167-6105(94)90091-4.

[33] Koblitz T, Bechmann A, Sogachev A, Sørensen N, Réthoré PE. Computational Fluid Dynamics model of stratified atmospheric boundary-layer flow. Wind Energy 2015; 18:75–89. https://doi.org/10.1002/we.1684.

[34] Kosović B, Curry JA. A large eddy simulation study of a quasi-steady, stably stratified atmospheric boundary layer. J Atmos Sci 2000;57(8):1052–68. https://doi.org/10.1175/1520-0469(2000)057<1052:ALESSO>2.0.CO;2.

[35] Lang S, McKeogh E. LIDAR and SODAR measurements of wind speed and direction in upland terrain for wind energy purposes. Rem Sens 2011;3(9):1871–901. https://doi.org/10.3390/rs3091871.

[36] Lenschow DH, Li XS, Zhu CJ, Stankov BB. The stably stratified boundary layer over the Great Plains. Boundary-Layer Meteorol 1988;42:95–121. https://doi.org/10.1007/BF00119877.

[37] Li T, Liu Z, Wang H, Bian W, Yang Q. Large eddy simulation for the effects of ground roughness and atmospheric stratification on the wake characteristics of wind turbines mounted on complex terrains. Energy Convers Manage 2022;268: 115977. https://doi.org/10.1016/j.enconman.2022.115977.

[38] Liu L, Stevens RJ. Effects of atmospheric stability on the performance of a wind turbine located behind a three-dimensional hill. Renew Energy 2021;175:926–35. https://doi.org/10.1016/j.renene.2021.05.035.

[39] Liu Z, Cao S, Liu H, Ishihara T. Large-eddy simulations of the flow over an isolated three-dimensional hill. Boundary-Layer Meteorol 2019;170:415–41. https://doi.org/10.1007/s10546-018-0410-2.

[40] Liu Z, Diao Z, Ishihara T. Study of the flow fields over simplified topographies with different roughness conditions using large eddy simulations. Renew Energy 2019; 136:968–92. https://doi.org/10.1016/j.renene.2019.01.032.

[41] Liu Z, Ishihara T, He X, Niu H. LES study on the turbulent flow fields over complex terrain covered by vegetation canopy. J Wind Eng Ind Aerod 2016;155:60–73. https://doi.org/10.1016/j.jweia.2016.05.002.

[42] Liu Z, Ishihara T, Tanaka T, He X. LES study of turbulent flow fields over a smooth 3-D hill and a smooth 2-D ridge. J Wind Eng Ind Aerod 2016;153:1–12. https://doi.org/10.1016/j.jweia.2016.03.001.

[43] Liu Z, Li W, Shen L, Han Y, Zhu Z, Hua X. Numerical study of stable stratification effects on the wind over simplified tall building models using large-eddy simulations. Build Environ 2021;193:107625. https://doi.org/10.1016/j.buildenv.2021.107625.

[44] Loureiro JB, Alho AT, Freire APS. The numerical computation of near-wall turbulent flow over a steep hill. J Wind Eng Ind Aerod 2008;96(5):540–61. https://doi.org/10.1016/j.jweia.2008.01.011.

[45] Lu B, Li Q. Influence of atmospheric stability on air ventilation and thermal stress in a compact urban site by large eddy simulation. Build Environ 2022;216:109049. https://doi.org/10.1016/j.buildenv.2022.109049.

[46] Lun YF, Mochida A, Murakami S, Yoshino H, Shirasawa T. Numerical simulation of flow over topographic features by revised k-ε models. J Wind Eng Ind Aerod 2003; 91(1–2):231–45. https://doi.org/10.1016/S0167-6105(02)00348-3.

[47] Mason PJ, King JC. Atmospheric flow over a succession of nearly two-dimensional ridges and valleys. Q J R Meteorol Soc 1984;110(466):821–45. https://doi.org/10.1002/qj.49711046604.

[48] Menke R, Vasiljević N, Wagner J, Oncley SP, Mann J. Multi-lidar wind resource mapping in complex terrain. Wind Energy Sci 2020;5(3):1059–73. https://doi.org/10.5194/wes-5-1059-2020.

[49] Meroney RN. Fluid dynamics of flow over hills and mountains: insights obtained through physical modeling (Chapter 7). Monograph of atmospheric processes over complex terrain. Boston, Massachusetts: Am. Meteorol. Soc; 1990. p. 145–72. https://doi.org/10.1007/978-1-935704-25-6_7.

[50] Neff DE, Meroney RN. Wind-tunnel modeling of hill and vegetation influence on wind power availability. J Wind Eng Ind Aerod 1998;74:335–43. https://doi.org/10.1016/S0167-6105(98)00030-0.

[51] Nieuwstadt FT. The turbulent structure of the stable, nocturnal boundary layer. J Atmos Sci 1984;41(14):2202–16. https://doi.org/10.1175/1520-0469(1984)041<2202:TTSOTS>2.0.CO;2.

[52] Ohya Y, Uchida T. Turbulence structure of stable boundary layers with a near-linear temperature profile. Boundary-Layer Meteorol 2003;108:19–38. https://doi.org/10.1023/A:1023069316164.

[53] Ohya Y, Uchida T. Laboratory and numerical studies of the convective boundary layer capped by a strong inversion. Boundary-Layer Meteorol 2004;112:223–40. https://doi.org/10.1023/B:BOUN.0000027913.22130.73.

[54] Ohya Y, Uchida T. Laboratory and numerical studies of the atmospheric stable boundary layers. J Wind Eng Ind Aerod 2008;96(10–11):2150–60. https://doi.org/10.1016/j.jweia.2008.02.037.

[55] Pearse JR, Lindley D, Stevenson DC. Wind flow over ridges in simulated atmospheric boundary layers. Boundary-Layer Meteorol 1981;21:77–92. https://doi.org/10.1007/BF00119369.

[56] Qian GW, Song YP, Ishihara T. A control-oriented large eddy simulation of wind turbine wake considering effects of Coriolis force and time-varying wind conditions. Energy 2022;239:121876. https://doi.org/10.1016/j.energy.2021.121876.

[57] Radünz WC, Sakagami Y, Haas R, Petry AP, Passos JC, Miqueletti M, Dias E. The variability of wind resources in complex terrain and its relationship with atmospheric stability. Energy Convers Manage 2020;222:113249. https://doi.org/10.1016/j.enconman.2020.113249.

[58] Radünz WC, Sakagami Y, Haas R, Petry AP, Passos JC, Miqueletti M, Dias E. Influence of atmospheric stability on wind farm performance in complex terrain. Appl Energy 2021;282:116149. https://doi.org/10.1016/j.apenergy.2020.116149.

[59] Ross AN, Arnold S, Vosper SB, Mobbs SD, Dixon N, Robins AG. A comparison of wind-tunnel experiments and numerical simulations of neutral and stratified flow

over a hill. Boundary-Layer Meteorol 2004;113:427–59. https://doi.org/10.1007/s10546-004-0490-z.
[60] Santos P, Mann J, Vasiljević N, Cantero E, Sanz Rodrigo J, Borbón F, et al. The Alaiz experiment: untangling multi-scale stratified flows over complex terrain. Wind Energy Sci 2020;5(4):1793–810. https://doi.org/10.5194/wes-5-1793-2020.
[61] Sathe A, Mann J, Barlas T, Bierbooms WAAM, Van Bussel GJW. Influence of atmospheric stability on wind turbine loads. Wind Energy 2013;16(7):1013–32. https://doi.org/10.1002/we.1528.
[62] Smedman AS. Observations of a multi-level turbulence structure in a very stable atmospheric boundary layer. Boundary-Layer Meteorol 1988;44(3):231–53. https://doi.org/10.1007/BF00116064.
[63] Strickland JM, Gadde SN, Stevens RJ. Wind farm blockage in a stable atmospheric boundary layer. Renew. Energy. 2022;197:50–8. https://doi.org/10.1016/j.renene.2022.07.108.
[64] Takahashi T, Ohtsu T, Yassin MF, Kato S, Murakami S. Turbulence characteristics of wind over a hill with a rough surface. J Wind Eng Ind Aerod 2002;90(12–15):1697–706. https://doi.org/10.1016/S0167-6105(02)00280-5.
[65] Tamura T, Cao S, Okuno A. LES study of turbulent boundary layer over a smooth and a rough 2D hill model. Flow Turbul Combust 2007;79:405–32. https://doi.org/10.1016/B978-008044544-1/50024-8.
[66] Tamura T, Okuno A, Sugio Y. LES analysis of turbulent boundary layer over 3D steep hill covered with vegetation. J Wind Eng Ind Aerod 2007;95(9–11):1463–75. https://doi.org/10.1016/j.jweia.2007.02.014.
[67] Taylor PA, Teunissen HW. The Askervein Hill project: overview and background data. Boundary-Layer Meteorol 1987;39:15–39. https://doi.org/10.1007/BF00121863.
[68] Thordal MS, Bennetsen JC, Koss HHH. Review for practical application of CFD for the determination of wind load on high-rise buildings. J Wind Eng Industr Aerodyn 2019;186:155–68. https://doi.org/10.1016/j.jweia.2018.12.019.
[69] Uchida T, Takakuwa S. Numerical investigation of stable stratification effects on wind resource assessment in complex terrain. Energies 2020;13(24):6638. https://doi.org/10.3390/en13246638.
[70] Van Ulden AP, Wieringa J. Atmospheric boundary layer research at Cabauw. Boundary-Layer Meteorol 1996;78:39–69. https://doi.org/10.1007/BF00122486.
[71] Wan F, Porté-Agel F. Large-eddy simulation of stably-stratified flow over a steep hill. Boundary-Layer Meteorol 2011;138:367–84. https://doi.org/10.1007/s10546-010-9562-4.
[72] Wharton S, Newman JF, Qualley G, Miller WO. Measuring turbine inflow with vertically-profiling lidar in complex terrain. J Wind Eng Ind. Aerod 2015;142:217–31. https://doi.org/10.1016/j.jweia.2015.03.023.
[73] Wu X. Inflow turbulence generation methods. Annu Rev Fluid Mech 2017;49(1):23–49. https://doi.org/10.1146/annurev-fluid-010816-060322.
[74] Yamaguchi A, Tavana A, Ishihara T. Assessment of wind over complex terrain considering the effects of topography, atmospheric stability and turbine wakes. Atmosphere (Basel) 2024;15(6):723. https://doi.org/10.3390/atmos15060723.
[75] Yan BW, Li QS, He YC, Chan PW. RANS simulation of neutral atmospheric boundary layer flows over complex terrain by proper imposition of boundary conditions and modification on the k-ε model. Environ Fluid Mech 2016;16(1):1–23. https://doi.org/10.1007/s10652-015-9408-1.
[76] Yang Q, Zhou T, Yan B, Liu M, Van Phuc P, Shu Z. LES study of topographical effects of simplified 3D hills with different slopes on ABL flows considering terrain exposure conditions. J Wind Eng Ind Aerod 2021;210:104513. https://doi.org/10.1016/j.jweia.2020.104513.
[77] Zhang W, Markfort CD, Porté-Agel F. Wind-tunnel experiments of turbulent wind fields over a two-dimensional (2D) steep hill: effects of the stable boundary layer. Boundary-Layer Meteorol 2023:1–21. https://doi.org/10.1007/s10546-023-00820-2.
[78] Zhou T, Yan B, Yang Q, Hu W, Chen F. POD analysis of spatiotemporal characteristics of wake turbulence over hilly terrain and their relationship to hill slope, hill shape and inflow turbulence. J Wind Eng Ind. Aerod 2022;224:104986. https://doi.org/10.1016/j.jweia.2022.104986.